

# Bidirectional Zero Poisson's Ratio Elastomers with Self-Deformable Soft Mechanical Metamaterials for Stretchable Displays

Jun-Chan Choi, Hoon Yeub Jeong, Jae-Hong Sun, Junghwan Byun, Jeongtaek Oh, Seok Joon Hwang, Phillip Lee, Dong Won Lee, Jeong Gon Son, Seunghyun Lee,\* and Seungjun Chung\*

Stretchable displays, capable of reversible expansion, represent significant advancements in free-form display technologies. However, the high Poisson's ratio ( $\nu$ ) of elastomer substrates leads to unintended deformation under tensile strain, resulting in image warping. To address this, a meta-elastomer (ME) substrate with a bidirectional zero  $\nu$ , incorporating a self-deformable soft mechanical metamaterial (MM) frame, is introduced. The  $\nu$  of the ME is precisely programmed by the interaction between the deformation of the MM frame, which exhibits a negative  $\nu$ , and the elastomer matrix, which has a positive  $\nu$ . The soft MM frame, stiffer than the elastomer matrix, undergoes both structural deformation and length alteration during substrate tensile strain. This synergistic effect enables achieving a nearly bidirectional zero  $\nu$ , thus overcoming the limitations of conventional tessellated rigid MM composites. Furthermore, the ME substrate, which is chemically cross-linked at the junction interface, demonstrates exceptional mechanical robustness, enduring over 180% stretching and more than 10 000 cycles. By counteracting the Poisson's effect, the ME substrate with an integrated pixel array ensures translational pixel movement along the tensile axis during bidirectional stretching, minimizing undesired pixel movement in other directions. The stretchable ME presents key advancements for implementing more stable and reliable stretchable display applications.

## 1. Introduction

The emergence of the Internet of Everything era has led to display technology becoming indispensable across various aspects of our lives, such as smart homes, automotive industries, and wearable devices.<sup>[1–6]</sup> This evolution necessitates displays in diverse forms, tailored to specific environments and objectives, underscoring the need for innovative device form factors. To this end, flexible displays on thin plastic substrates have been commercialized, and foldable and rollable displays have been introduced, allowing users to adjust screen size on demand.<sup>[7,8]</sup> Recently, the focus has shifted toward stretchable displays, which can deliver visual information in both static and dynamic unrestricted forms, leading to significant innovation in display form factors.<sup>[9–12]</sup>

Research on stretchable substrate materials has become a priority with the increasing diversity of display form factors. For the practical applicability of stretchable displays, stretchable substrates must

J.-C. Choi, H. Y. Jeong, S. Chung  
School of Electrical Engineering  
Korea University  
Seoul 02841, Republic of Korea  
E-mail: [seungjun@korea.ac.kr](mailto:seungjun@korea.ac.kr)

J.-C. Choi, H. Y. Jeong, J.-H. Sun, J. Byun, J. G. Son  
Soft Hybrid Materials Research Center  
Korea Institute of Science and Technology  
Seoul 02792, Republic of Korea

 The ORCID identification number(s) for the author(s) of this article can be found under <https://doi.org/10.1002/adfm.202406725>

© 2024 The Author(s). Advanced Functional Materials published by Wiley-VCH GmbH. This is an open access article under the terms of the [Creative Commons Attribution-NonCommercial-NoDerivs License](#), which permits use and distribution in any medium, provided the original work is properly cited, the use is non-commercial and no modifications or adaptations are made.

DOI: 10.1002/adfm.202406725

J. Oh, S. Lee  
Department of Mechanical System Design Engineering  
Seoul National University of Science and Technology  
Seoul 01811, Republic of Korea  
E-mail: [s.lee@seoultech.ac.kr](mailto:s.lee@seoultech.ac.kr)

S. J. Hwang, P. Lee  
Advanced Photovoltaics Research Center  
Korea Institute of Science and Technology  
Seoul 02792, Republic of Korea

S. J. Hwang, P. Lee  
Division of Nano and Information Technology  
University of Science and Technology  
Seoul 02792, Republic of Korea

D. W. Lee, J. G. Son  
KU-KIST Graduate School of Converging Science and Technology  
Korea University  
Seoul 02841, Republic of Korea

maintain stable tensile and recovery functions under strains exceeding 30%.<sup>[13]</sup> Early studies in this field employed buckling or Kirigami designs to introduce stretchability into plastic substrates;<sup>[14–16]</sup> however, these structure-dependent approaches encountered mechanical and optical challenges, such as limited resolution and image blurring. With the recent advancements in low-temperature processing technology, elastomer materials with inherent stretchability have gained significant attention as substrate materials to overcome the limitations of structured plastic substrates.<sup>[17–20]</sup> Nonetheless, the high Poisson's ratio ( $\nu$ ) of elastomers remains a significant challenge, leading to image distortion regardless of the tensile direction.<sup>[21]</sup>

$\nu$ , defined as the negative ratio of transverse strain ( $\epsilon_{\text{trans}}$ ) to axial strain ( $\epsilon_{\text{axial}}$ ), indicates the degree of lateral expansion or compression a material undergoes under external load.<sup>[22]</sup> Elastomers, known for their wide range of moduli ( $E$ ) spanning from kilopascals (kPa) to megapascals (MPa), consistently exhibit  $\nu$  approaching 0.5, regardless of the tensile direction.<sup>[23]</sup> This indicates that the image on a display fabricated on elastomer substrates is distorted perpendicular to the tensile direction. To mitigate image warping issues caused by unwanted substrate deformation due to the Poisson's effect and to ensure predictable translational pixel movement under stretching in various directions for practical display applications, it would be beneficial to have a  $\nu$  of 0 for stretchable substrates, but challenges remain in terms of materials and processing.

In this study, we propose a solution through a meta-elastomer (ME) substrate with a bidirectional zero  $\nu$ , which is obtained by integrating a self-deformable soft mechanical metamaterial (MM) frame within an elastomer matrix. MMs, which are artificial materials endowed with unique mechanical properties, can be customized through designed structures to exhibit specific characteristics, such as a negative  $\nu$ .<sup>[24,25]</sup> By embedding a soft MM frame with negative  $\nu$  into an elastomer matrix with a positive  $\nu$ , we create a distinctive composite substrate system with a bidirectional zero  $\nu$ . As the ME substrate stretches, the soft MM frame not only undergoes structural folding and unfolding but also induces inherent length changes in each rib according to the tensile axis. This allows for independent transformations along the  $x$ - $y$  tensile axes, achieving a bidirectional zero  $\nu$ . Finite element method (FEM) simulations were employed to design the soft MM frame and analyze the ME substrate's  $\nu$  under various modulus conditions between the frame and matrix. This design strategy facilitated a near-zero  $\nu$  ( $-0.1 < \nu < 0.1$ ) across the  $x$ - $y$  axes within a 30% tensile range, which was attained through the interaction between the expansion of the soft MM frame and the contraction of the elastomer matrix. Additionally, introducing transparent heterogeneously modulus-engineered elastomers with similar refractive indices for the frame and matrix resulted in high transmittance without ray distortion owing to light refraction. Chemical cross-linking between heterogeneous elastomer materials at the interface between the frame and matrix prevents delamination under high tensile conditions and minimizes hysteresis throughout repeated cycles. Finally, a linearly programmable displacement was demonstrated by the integrated light-emitting diode (LED) array in the ME substrate, under bidirectional stretching.

## 2. Results and Discussion

### 2.1. Self-Deformable Soft MM Design

**Figure 1a** illustrates the change in display images when a pristine elastomer (PE) with a Poisson's ratio ( $\nu$ ) of  $\approx 0.5$  and an ME with a near-zero  $\nu$  are used as substrates for stretchable displays. With the PE substrate, the display adopts a concave shape owing to the transverse contraction caused by the Poisson's effect during stretching, which results in image warping without translational movement of the display pixels. In contrast, the proposed ME substrate retains the rectangular shape during stretching as the expansion behavior of the self-deformable soft MM frame compensates for the contraction behavior of the elastomer matrix. This mechanism allows all display pixels on the substrate to undergo translational movement in the tensile direction, allowing predictable pixel displacement during substrate stretching. The display image does not warp during stretching, delivering for relatively accurate information compared to PE substrates. Additionally, since the pixel array maintains a rectangular shape, image adjustment and conversion via software are easier in practical applications.

To develop an ME substrate with a bidirectional zero  $\nu$ , we initially designed the shapes of MM structures with a negative  $\nu$ . Representative auxetic MM structures with negative  $\nu$  include re-entrant structures, chiral structures, and perforated sheets (Figure S1, Supporting Information).<sup>[26–28]</sup> The criteria guiding their incorporation into stretchable display substrates were as follows: 1) The MM frame must sustain a negative  $\nu$  across structural deformations within the target tensile range (0–30%), thereby ensuring a consistent  $\nu$  value regardless of the applied tensile strain. 2) Pixel displacement resulting from MM frame deformation should be predictable and linear. 3) For realizing bidirectional independent behaviors via different mechanisms, shape anisotropy across the  $x$ - $y$  axes was considered optimal. Considering these factors, an auxetic honeycomb configuration was chosen as the optimal MM frame structure.

A distinguishing feature of this study compared to existing research, is the introduction of a self-deformable soft MM frame. This frame induces not only structural folding and unfolding but also simultaneous inherent length changes in each rib according to the tensile axis during frame stretching. In contrast, conventional auxetic honeycomb-shaped rigid MM frames exhibit bidirectional connected deformation under frame stretching, and the  $\epsilon_{\text{axial}}$  of the unit cell can be defined as follows.

$$\epsilon_x = (\sin \theta_s / \sin \theta_0) - 1 \quad (1)$$

$$\epsilon_y = 2l_0 (\cos \theta_0 - \cos \theta_s) / h_0 \quad (2)$$

where  $l_0$ ,  $h_0$ ,  $\theta_0$ , and  $\theta_s$  denote the initial length of the inclined rib, the initial length of the straight rib, the initial angle between the inclined and straight ribs, and the angle between the inclined and straight ribs under uniaxial tensile deformation, respectively. During the MM frame stretching, the length of each rib is maintained constant, and the bidirectional strain ( $\epsilon_x$  and  $\epsilon_y$ ) and deformation pattern are determined by the  $\theta_0$  value (Figure 1b). For example, a rigid MM designed with a  $\theta_0$  of  $56.44^\circ$  displays  $\epsilon_{\text{axial}}$  of  $\approx 20\%$  and  $58\%$  along the  $x$  and  $y$  uniaxial stretching

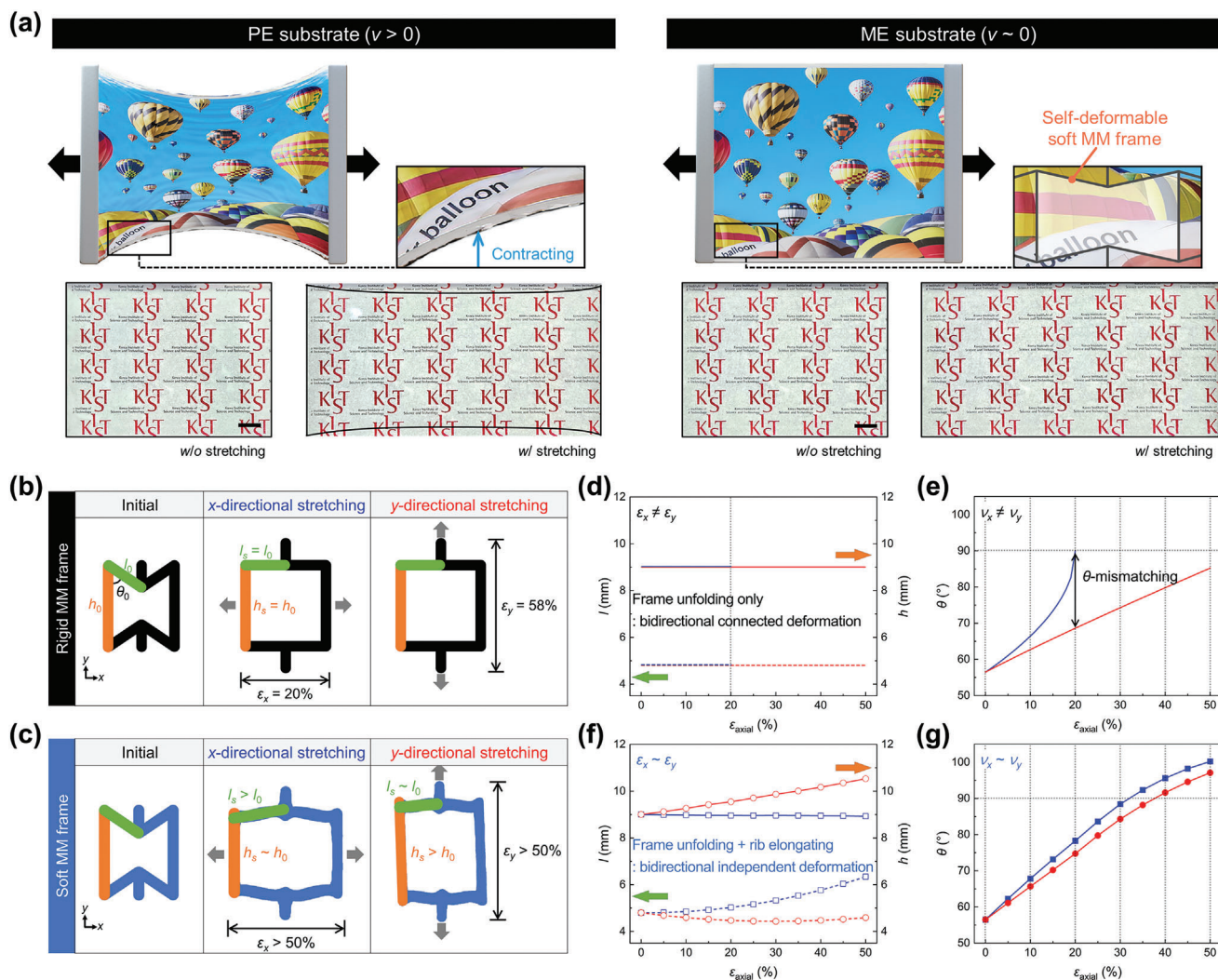


**Figure 1.** Self-deformable soft metamaterials (MM) for bidirectional zero  $\nu$  substrates in stretchable displays. a) Schematic and photographic images illustrating substrate deformation and display image changes under axial stretching of PE (positive  $\nu$ ) and ME (zero  $\nu$ ) substrates. Scale bar: 10 mm. b, c) Schematics of the unit cell deformation patterns of rigid and soft MM frames under bidirectional stretching along the  $x$ - $y$  axes. d–g) Variations in  $l_s$ ,  $h_s$ , and  $\theta_s$  according to the  $\epsilon_{axial}$  of (d, e) rigid MM frame (analytical curve fitting) and (f, g) soft MM frame (FEM simulation). The blue and red line graphs represent the cases of  $x$ -directional and  $y$ -directional stretching, respectively.

cases, respectively, when the structure is ideally fully unfolded (Figure 1d,e). Notably, when the MM frame is stretched along the  $x$ - $y$  axes, it exhibits bidirectional-connected structural deformations, resulting in a different  $\theta_s$  value, which is related to the bidirectional anisotropic  $\nu$  values, under the same  $\epsilon_{axial}$ .

Conversely, in soft MM composed of elastomers, structural deformation due to  $\theta$  is accompanied by changes in the lengths of  $l$  and  $h$ . In this case, the  $\epsilon_{axial}$  of the unit cell in the soft MM can be expressed as follows.

$$\epsilon_x = (l_s \sin \theta_s / l_0 \sin \theta_0) - 1 \quad (3)$$

$$\epsilon_y = \{h_s + 2(l_0 \cos \theta_0 - l_s \cos \theta_s) - h_0\} / h_0 \quad (4)$$

where  $l_s$  and  $h_s$  represent the deformed lengths of the inclined and straight ribs under tensile conditions, respectively (assuming linear elasticity,  $l_s = l_0(\sigma/E_{frame} + 1)$ ; here,  $\sigma$  is the effective stress

induced in the longitudinal direction of the frame).<sup>[29]</sup> During the tensile process, the soft MM frame facilitates simultaneous structural unfolding and length changes of the ribs, overcoming the  $\theta_0$ -dependent axial strain observed in traditional rigid MM frames (Figure 1b,c). Furthermore, inducing intrinsic elongation in each rib according to the tensile axis leads to bidirectional-independent frame transformations (Figure 1f). The bidirectional  $\nu$  of the soft MM frame was programmed through FEM simulation according to  $\theta_0$  by maintaining the modulus of the frame material and the ratio of  $l_0$  to  $h_0$  constant, and at  $\theta_0 = 56.44^\circ$ , the frame exhibited a similar negative  $\nu$  when uniaxially stretched along each of the  $x$  and  $y$  axes within the target tensile range (Figure S2, Supporting Information). At  $\theta_0 = 56.44^\circ$ , the soft MM frame exhibited a linear  $\theta_s$  graph according to  $\epsilon_{axial}$  within the target tensile range compared to the same rigid MM frame structure, with significantly reduced  $\theta_s$  variance along the  $x$ - $y$  tensile axis (Figure 1e,g). This indicates that when the soft

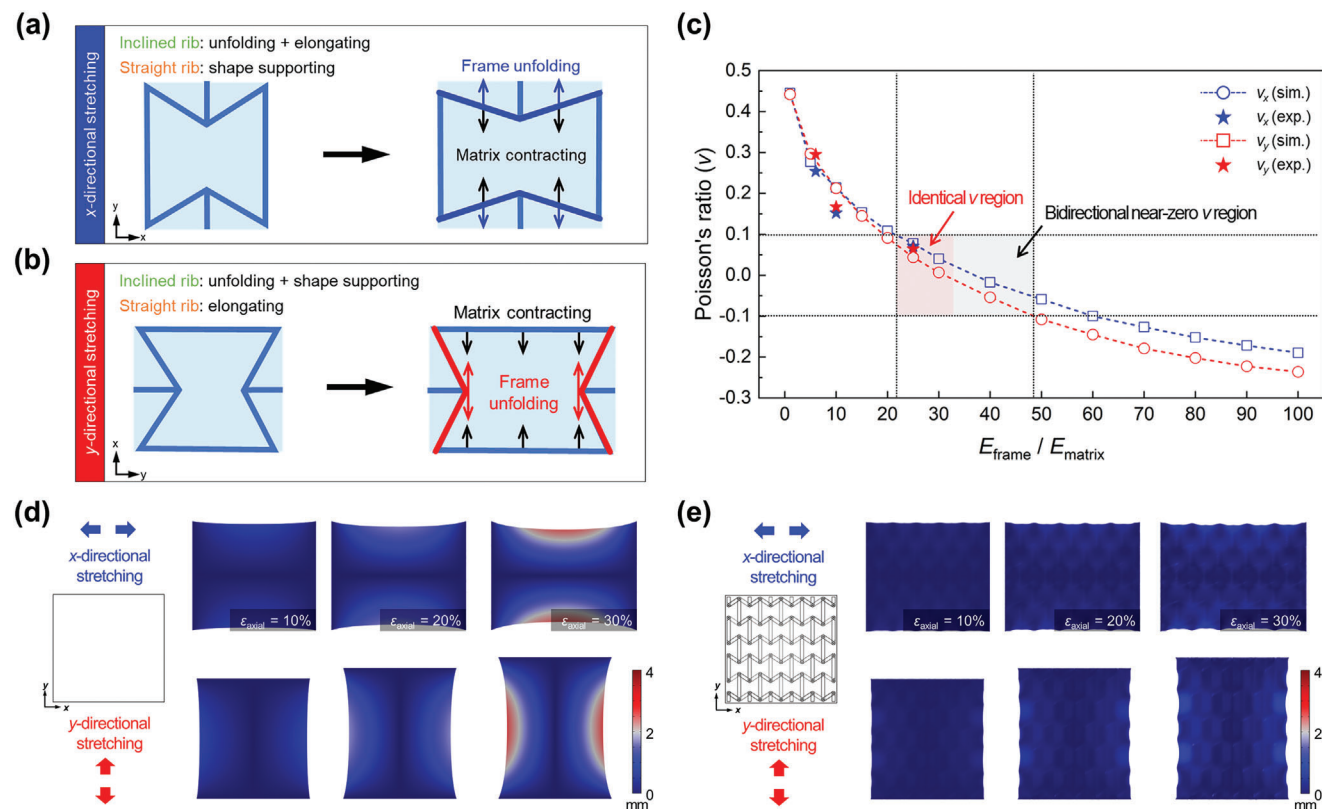


**Figure 2.** Modulus engineering of soft MM frame and elastomer matrix for bidirectional  $\nu$  programming. a,b) Mechanism for programming the  $\nu$  of ME substrates based on the interaction between MM frame expansion and elastomer matrix contraction during a) x-directional and b) y-directional stretching. c) FEM simulation and experimental results of the x–y bidirectional  $\nu$  in relation to the ratio of  $E_{\text{frame}}$  and  $E_{\text{matrix}}$ . d,e) Transverse strain maps under bidirectional stretching for d) PE ( $E_{\text{frame}}/E_{\text{matrix}} = 1$ ) and e) ME ( $E_{\text{frame}}/E_{\text{matrix}} = 25$ ) substrates.

MM frame is stretched along each of the  $x$  and  $y$  axes, there is minimal variation in the  $\nu$  with the anisotropic behavior during uniaxial stretching, suggesting the potential for simultaneously controlling the bidirectional  $\nu$  when utilizing the soft MM frame as a component of a stretchable ME substrate (Figure S3, Supporting Information).

## 2.2. Modulus Engineering Between Soft MM Frame and Matrix

The bidirectional  $\nu$  of the ME substrate can be programmed by controlling the competitive effects between the expansion behavior of the soft MM frame and the contraction behavior of the elastomer matrix. To realize the ME substrate, an elastomer MM frame, designed via direct ink writing (DIW), was integrated into the elastomer matrix. The optimal ratio between the thickness of the MM frame and the upper/lower surrounding layers, which ensures sufficient momentum for frame expansion, was determined to be 8:3 (Figure S4, Supporting Information). When the ME substrate is stretched along the  $x$ -axis,  $\nu_x$  is determined by the expansion of the frame, induced by both structural deformation and the lengthening of the inclined ribs of the soft MM frame by competing with the contraction behavior of the elastomer matrix (Figure 2a). Conversely, when the ME substrate is elongated along the  $y$ -axis, the straight ribs of the frame are stretched, leading to structural deformation in the inclined ribs, with  $\nu_y$  sim-

ilarly determined through the competitive interaction between frame expansion and matrix contraction (Figure 2b). Therefore, owing to the length changes of the ribs according to the tensile axis, the stretching of the ME substrate occurs independently along the  $x$  and  $y$  axes. To achieve a bidirectional zero  $\nu$  within the target tensile range (0–30%), it is crucial to design the modulus variation between the MM frame ( $E_{\text{frame}}$ ) and the matrix ( $E_{\text{matrix}}$ ) to control the complex behaviors of expansion and contraction.

Bidirectional  $\nu$  under a 30%  $\epsilon_{\text{axial}}$  condition was evaluated by FEM simulations, focusing on the  $E_{\text{frame}}$  to  $E_{\text{matrix}}$  ratio of the stretchable ME substrate (Figure 2c). A PE substrate ( $E_{\text{frame}}/E_{\text{matrix}} = 1$ ) exhibited a  $\nu$  value close to 0.45 along both the  $x$  and  $y$  axes. As the  $E_{\text{frame}}/E_{\text{matrix}}$  increased,  $\nu$  consistently decreased along both tensile axes. When  $E_{\text{frame}}/E_{\text{matrix}}$  was less than 10,  $\nu_x$  was lower than  $\nu_y$  because the vertically aligned straight ribs restricted the matrix's contraction during x-directional stretching. The values of  $\nu_x$  and  $\nu_y$  reversed when  $E_{\text{frame}}/E_{\text{matrix}}$  exceeded 10, and a  $\nu$  value close to zero ( $-0.1 < \nu < 0.1$ ) was achieved in both tensile directions when  $E_{\text{frame}}/E_{\text{matrix}}$  ranged between 22 and 48 (Figure 2c, gray area). For practical stretchable device applications, achieving similar  $\nu$  along both tensile axes is desirable, and it was observed that the variance between  $\nu_x$  and  $\nu_y$  is minimal when  $E_{\text{frame}}/E_{\text{matrix}}$  ranges from 22 to 33 (Figure 2c, red area). Strain maps generated through FEM simulations for both PE ( $E_{\text{frame}}/E_{\text{matrix}} = 1$ ) and ME ( $E_{\text{frame}}/E_{\text{matrix}} = 25$ ) substrates showed that the expansion of the soft MM

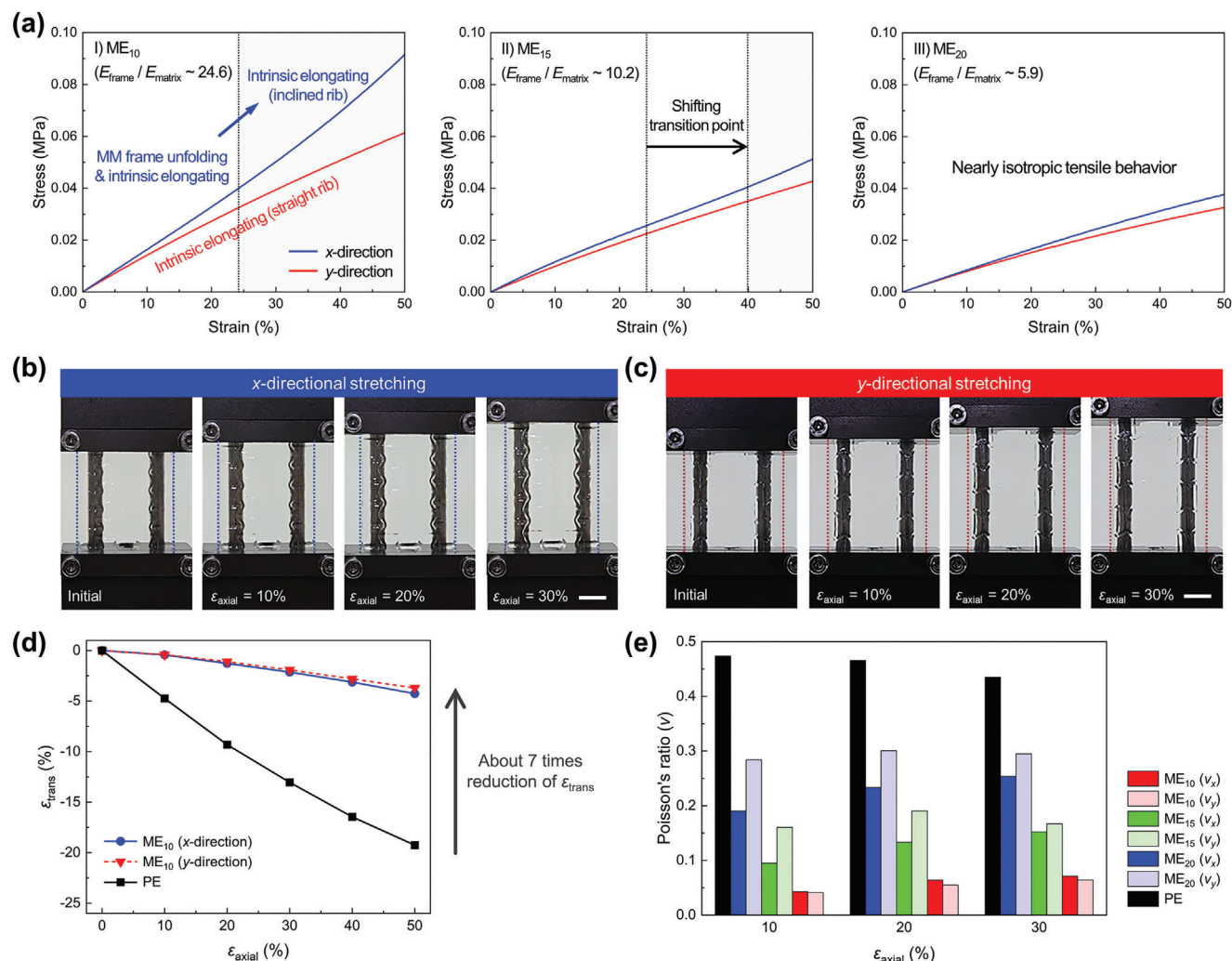


**Figure 3.** Bidirectional stress–strain behavior and  $\nu$  of ME substrates. a) Stress–strain curves for I) ME<sub>10</sub> ( $E_{\text{frame}}/E_{\text{matrix}} \approx 24.6$ ), II) ME<sub>15</sub> ( $E_{\text{frame}}/E_{\text{matrix}} \approx 10.2$ ), and III) ME<sub>20</sub> ( $E_{\text{frame}}/E_{\text{matrix}} \approx 5.9$ ) substrates. b,c) Photographic images of the ME<sub>10</sub> substrate under b) x-directional and c) y-directional stretching conditions. Scale bar: 10 mm. d)  $\epsilon_{\text{trans}}$  as a function of  $\epsilon_{\text{axial}}$  for PE and ME<sub>10</sub>. e) Bidirectional  $\nu$  for each stretchable substrate, shown alongside  $\epsilon_{\text{axial}}$ .

frame during uniaxial stretching along the  $x$  and  $y$  axes effectively suppresses the contraction of the elastomer matrix due to the Poisson's effect, ensuring bidirectional uniform deformation with the anisotropic behavior (Figure 2d,e). The ME substrate, designed with optimal modulus variation ( $E_{\text{frame}}/E_{\text{matrix}} = 25$ ), demonstrated sufficient suppression of transverse contraction across the entire target tensile strain range from 0% to 30%, aiming to achieve a bidirectional zero  $\nu$ .

### 2.3. Bidirectional Zero $\nu$ of ME Substrates

Based on the structural design of the MM frame and modulus engineering between the frame and matrix, polydimethylsiloxane (PDMS) with different moduli was selected for the frame and matrix to experimentally implement an ME substrate with bidirectional zero  $\nu$ . PDMS is one of the most promising silicon elastomers for stretchable substrates, due to its remarkable

stretchability, thermal stability, and optical clarity.<sup>[30,31]</sup> The customization of its elastic modulus is straightforward, achieved by adjusting the base-to-curing agent ratio. We employed PDMS with varying base-to-agent ratios: P<sub>40</sub> ( $E = 0.05$  MPa) for the matrix and higher modulus materials, P<sub>10</sub> ( $E = 1.23$  MPa), P<sub>15</sub> ( $E = 0.51$  MPa), and P<sub>20</sub> ( $E = 0.29$  MPa), for the frame to explore the influence of frame modulus ( $E_{\text{frame}}$ ) on the tensile deformation of the ME substrate (Figure S5, Supporting Information). For the ME<sub>10</sub> substrate, which pairs the P<sub>10</sub> frame and P<sub>40</sub> matrix ( $E_{\text{frame}}/E_{\text{matrix}} \approx 24.6$ ), we observed simultaneous structural alterations and length changes of the inclined ribs during  $x$ -axis stretching. This resulted in a gradual increase in the slope of the stress–strain curve under axial strain reflecting the alignment characteristics of the inclined ribs in the tensile direction (Figure 3a,I; Figure S6a, Supporting Information). Notably, beyond 25% axial strain, a significant change in the slope indicated that length elongation of the inclined ribs predominantly dictated the tensile behavior of the ME substrate. Conversely, when

stretching the ME<sub>10</sub> substrate along the  $y$ -axis, the straight ribs were elongated and the inclined ribs deformed independently, maintaining a linear stress–strain curve without slope transition within the targeted tension range. For the ME<sub>15</sub> substrate ( $E_{\text{frame}}/E_{\text{matrix}} \approx 10.2$ ), employing P<sub>15</sub> as the frame material, the effect of MM frame expansion on the overall substrate deformation decreased compared to the ME<sub>10</sub> substrate, evidently observed as the slope transition point of the stress–strain curve shifted to a higher axial strain value beyond 25% during  $x$ -axis stretching (Figure 3a,II; Figure S6b, Supporting Information). The ME<sub>20</sub> substrate, with an  $E_{\text{frame}}/E_{\text{matrix}}$  of merely 5.9, exhibited minimal deviation in the two stress–strain curves when stretched in the  $x$  and  $y$  directions, demonstrating almost isotropic tensile behavior akin to that of the PE substrate (Figure 3a,III; Figure S6c, Supporting Information).

Figure 3b,c shows the experimental bidirectional tensile deformation of the ME<sub>10</sub> substrate. The inherent contraction behavior of the matrix, driven by the Poisson's effect, is effectively counterbalanced by the integrated soft MM frame, which maintains the rectangular shape of the substrate throughout the stretching process. FEM simulations performed to analyze the stress profile of the ME substrate during bidirectional stretching revealed that stress concentrations vary along distinct ribs according to the direction of tension, facilitating frame deformation (Figure S7, Supporting Information). Furthermore, the stress distribution, influenced by the designed modulus contrast between each area of the frame and matrix, played a pivotal role in determining the bidirectional  $\nu$  of the ME substrates. Quantitative analysis of the induced  $\epsilon_{\text{trans}}$  during the stretching of the ME<sub>10</sub> substrate in the  $x$  and  $y$  directions revealed that it remained linear across the entire target  $\epsilon_{\text{axial}}$  range of 0% to 30% (Figure 3d). This linearity indicates an approximately sevenfold reduction in  $\epsilon_{\text{trans}}$  compared to the PE substrate, resulting in  $\nu$  values of 0.07 and 0.06 for the  $x$  and  $y$  directions, respectively. The experimentally determined bidirectional  $\nu$  of the ME<sub>10</sub> substrate well-matched the FEM simulation results, maintaining a near-zero constant value across the entire tensile range, regardless of the stretching direction (Figures 2c and 3e; Table S1, Supporting Information). Achieving bidirectional  $\nu$  values of 0.07 and 0.06 in the ME<sub>10</sub> substrate highlights the significant potential in improving image warping caused by the Poisson's effect in display applications, a challenge for conventional stretchable substrate materials.

## 2.4. Optical and Mechanical Characteristics of ME for Display Applications

To leverage the ME substrate with bidirectional zero  $\nu$  for diverse display technologies, it is essential to achieve high transparency and prevent ray distortion caused by light refraction through the substrate. The ME<sub>10</sub> substrate, constructed using PDMS for both its frame and matrix, demonstrated exceptional optical properties in the visible spectrum. Given that the P<sub>10</sub> and P<sub>40</sub> components are produced from the same PDMS monomer, the negligible refractive index difference between them—less than 0.0016 in the visible spectrum—significantly reduced ray distortion at the interface between the frame and matrix (Figure S8, Supporting Information). Consequently, the

ME<sub>10</sub> substrate not only ensured a transmittance rate of 91% in the visible spectrum but also retained an angular luminance profile similar to that of conventional PE substrates (Figure 4a,b; Figure S9, Supporting Information). Furthermore, the ME<sub>10</sub> substrate successfully transmitted clear images across a wide range of brightness levels, from low intensity (280 cd m<sup>-2</sup>) to high intensity (1120 cd m<sup>-2</sup>), without hindering visible MM frame structures or blur (Figure 4c). Comparative analysis of the optical properties of conventional display substrates (glass and plastic films) revealed that the ME<sub>10</sub> substrate has similar transmission characteristics in the visible light range and produces comparable display images through the substrate (Figures S10 and S11, Supporting Information). This demonstrates the ME<sub>10</sub> substrate's compatibility with display applications, effectively maintaining image clarity under various backlight conditions.

Leveraging materials derived from the same monomer for both the frame and the matrix facilitates the sharing of chemical bonding groups at the boundary interfaces. When fabricating the ME substrate, the MM frame undergoes an initial soft cure to maintain its form after printing, followed by a full cure once it is embedded within the matrix. This method allows for chain inter-diffusion at the interface, leading to the creation of additional siloxane (Si–O–Si) bonds.<sup>[32,33]</sup> Consequently, this process yields a superior interfacial bonding strength to that of typical composite systems (Figure S4, Supporting Information). The lower modulus of the proposed MM frame than traditional polymeric MM frames plays a crucial role in reducing the stress differences at the frame-matrix interface during stretching, thereby decreasing stress concentration (Figure S12, Supporting Information). This enhanced bonding and diminished stress concentration ensure the reliability of the ME substrate, preventing delamination or structural damage even at high bidirectional tensile strains of 180% (Figure 4d). Additionally, in cyclic testing, introducing a highly cross-linked MM frame that limits polymer chain mobility within the matrix significantly reduced viscoelastic loss and decreased hysteresis (Figure 4e; Figure S13, Supporting Information). At a 30% bidirectional strain, the substrate exhibited a minimal stress variation rate of 8% over 10 000 testing cycles, representing a substantial advancement in performance relative to conventional PE substrates.

To deploy a mechanically and optically optimized ME substrate for stretchable displays effectively, pixels must maintain a linear and predictable path during bidirectional stretching. To support this behavior, we placed a 5 × 5 micro-LED array on both PE and ME<sub>10</sub> stretchable substrates. To ensure stable electrical connections during stretching, each LED was connected with arched copper wires, and an adhesive layer was introduced underneath the LEDs to enhance bonding between the LEDs and the substrates (Figure S14, Supporting Information). The LED array on the PE substrate experienced pixel displacement not only along the tensile axis but also toward the center due to the Poisson's effect, resulting in a concave rearrangement that does not maintain the rectangular array (Figure 5). In contrast, the LED array on the ME<sub>10</sub> substrate minimized pixel displacement toward the center, showing linear pixel movement along the tensile axis, maintaining predictable and uniform pixel displacement in both  $x$  and  $y$  directions. Experimental analysis of the

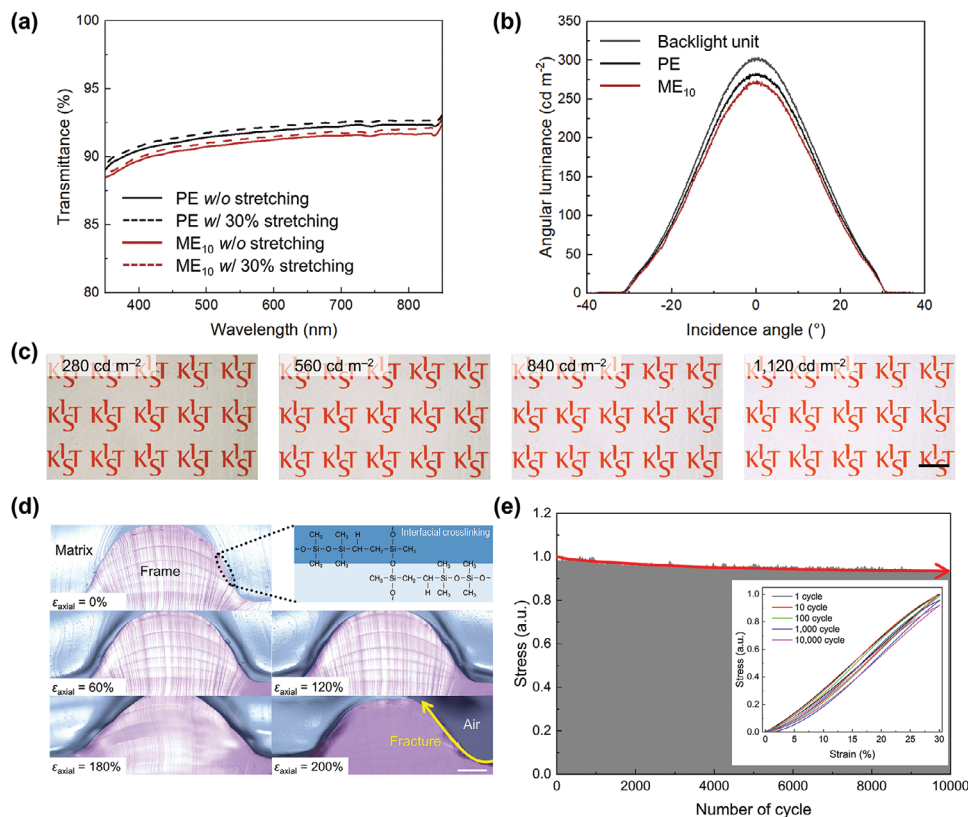


**Figure 4.** Optical properties and mechanical reliability. a) Transmittance of PE and ME<sub>10</sub> across the visible spectral range. b) Angular luminance as a function of the light incidence angle on the stretchable substrates. c) Images transmitted through the ME<sub>10</sub> under conventional display brightness conditions. Scale bar: 10 mm. d) Cross-sectional optical microscope images of the frame and matrix regions of ME<sub>10</sub>, varying with  $\epsilon_{\text{axial}}$ . Scale bar: 0.25 mm. e) Stress variations in the ME<sub>10</sub> substrate under a 30% cyclic strain (inset: stress-strain curves of ME<sub>10</sub> for 1, 10, 100, 1000, and 10 000 cycles).

local  $\epsilon_{\text{axial}}$  and  $\epsilon_{\text{trans}}$  using digital image correlation (DIC) techniques showed that the PE substrate exhibited high  $\epsilon_{\text{trans}}$  and uneven strain distribution due to stress tailoring (Figure S15a, Supporting Information). In contrast, the ME<sub>10</sub> substrate exhibited very low  $\epsilon_{\text{trans}}$  and a relatively uniform strain distribution between

the edges and the center (Figure S15b, Supporting Information). These results highlight the reliability of the ME<sub>10</sub> substrate in preventing image warping, proving its utility in stretchable display applications where it is paramount to maintain image fidelity.

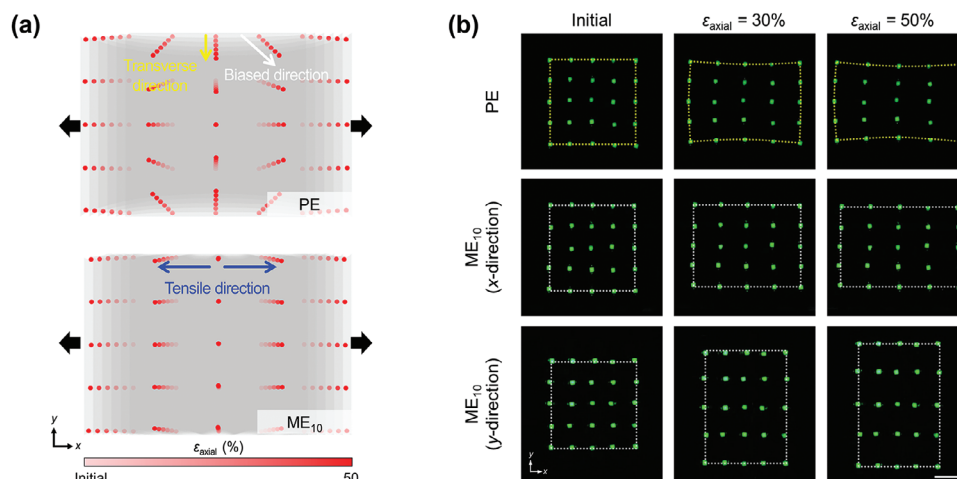


**Figure 5.** LED array pixel displacements under bidirectional stretching of substrates. a) FEM simulations and b) experimental results of LED array displacements mounted on PE and ME<sub>10</sub> substrates under uniaxial tensile strain. Scale bar: 10 mm.

### 3. Conclusion

In this study, a stretchable ME substrate that exhibits near-zero  $\nu$  in both  $x$  and  $y$  directions was developed by incorporating a self-deformable soft MM frame into an elastomer matrix. To address the challenges posed by intrinsically stretchable elastomer substrates, which have a high positive  $\nu$ , we optimized the design parameters and modulus variation of the MM frame and elastomer matrix through FEM simulations. Our approach allows the MM frame to undergo structural deformation and inherent elongation, which enables bidirectional independent tensile deformations. The effective regulation of  $\nu$  was achieved through the interaction between the MM frame's expansion (negative  $\nu$ ) and the elastomer matrix's contraction (positive  $\nu$ ) under tensile stress. The modulus ratio of the MM frame to elastomer matrix was  $\approx 24.6$ , demonstrating that the ME<sub>10</sub> substrate exhibited near-zero  $\nu$  values ( $\approx 0.07$  and  $0.06$  in the  $x$  and  $y$  directions, respectively) within a tensile strain range of 0–30%. Additionally, by matching the refractive indices of the MM frame and elastomer matrix, ray distortion could be minimized owing to refraction, and a high visible-light transmittance of  $\approx 91\%$  could be achieved. The stretchable ME substrate exhibited exceptional mechanical robustness up to 180% strain without structural failures, which can be attributed to the strong chemical bonding at the interface of the frame and matrix. Moreover, the MM frame drastically reduced viscoelastic loss in the elastomer matrix under repeated tensile stresses, showing a minimal stress change of 8% over 10 000 cycles at 30% tensile strain. Importantly, the LED pixel displacement on our ME substrate was precisely aligned with the tensile direction along both the  $x$  and  $y$  axes, effectively eliminating image warping by the Poisson's effect. Our stretchable ME presents key advancements for implementing more stable and reliable stretchable display applications, offering a novel approach to mitigate the challenges associated with the Poisson's effect in conventional stretchable platforms.

### 4. Experimental Section

**Fabrication of ME Substrates:** For the elastomer material used for both the frame and matrix, PDMS (Sylgard 184, Dow Corning) was utilized. The crosslinking density of the PDMS elastomer was controlled by mixing the base with the curing agent in ratios of 40:1 (P<sub>40</sub>), 20:1 (P<sub>20</sub>), 15:1 (P<sub>15</sub>), and 10:1 (P<sub>10</sub>), setting the Young's modulus of the material to  $\approx 0.05$ ,  $0.29$ ,  $0.51$ , and  $1.23$  MPa, respectively. A planetary centrifugal mixer (ARV-310, Thinky) was used at 2000 rpm for 5 min to achieve a bubble-free, uniform mixture. The elastomer mixtures were directly printed onto glass substrates using a programmable pneumatic dispenser (ML-808GX, Musashi Engineering) and a computer-controlled electric stage (SHOTmini200SX, Musashi Engineering). Initially, a 150- $\mu\text{m}$ -thick bottom layer of the P<sub>40</sub> mixture was printed and pre-baked at 100 °C for 10 min to fix its shape. Subsequently, an MM frame designed with computer-aided design software (AutoCAD 2020, Autodesk) was printed atop the bottom layer using the P<sub>10</sub>, P<sub>15</sub>, and P<sub>20</sub> mixtures. The auxetic-structured soft MM frame, with a thickness of 800  $\mu\text{m}$ , was created through 8-pass printing on a heating plate maintained at 100 °C. Finally, the P<sub>40</sub> mixture was dispensed to form a top-layer matrix with a thickness of 150  $\mu\text{m}$ , which was then fully cured in a baking oven at 100 °C for 10 h.

**Simulation Analysis:** FEM simulations were conducted using the structural module of COMSOL Multiphysics. The unit cells were meticulously designed based on specific geometric parameters:  $l_0 = 4.8$  mm,  $h_0 = 9$  mm, and  $\theta_0 = 56.44^\circ$ . The overall dimensions of the ME substrate were determined to be 33.4 mm by 34.5 mm, with a designated 0.5 mm gap

between the matrix and the frame at the substrate's edge. A fixed constraint was applied to one side of the matrix, while the opposite side was subjected to prescribed displacement conditions to induce stretching of the ME substrate. The strain was incrementally varied from 0% to 50%, in both the  $x$  and  $y$  stretching directions, maintaining zero displacement in the orthogonal directions. Subsequently, the von Mises stress within the matrix and the displacement of the ME in its stretched states were calculated. From these simulation outcomes, the  $\nu$  of the ME substrates were accurately evaluated post-stretching.

**Optical Characterization:** The refractive indices of PE films, prepared from a variety of PDMS mixtures (P<sub>10</sub>, P<sub>15</sub>, P<sub>20</sub>, and P<sub>40</sub>), were accurately measured at various visible wavelengths (404, 532, 633, and 829 nm) using a prism coupler (Model 2010/M, Metricon). To assess the visible light transmittance of both PE and ME substrates under 0% and 30% tensile strain, experiments were carried out with a stretching jig in conjunction with a UV-vis spectrometer (V-600, Jasco). The transmittance characteristics of these elastomers were thoroughly analyzed across the wavelength range of 350–850 nm, under both 0% and 30% tensile strain conditions, using the same stretching jig and UV-vis spectrometry. To compare the optical properties with those of the transparent substrate materials used in conventional displays, such as soda-lime glass, polyethylene naphthalate (PEN, Dupont) film, and clear polyimide (cPI, Kolon) film, the transmission characteristics using UV-vis spectroscopy over the wavelength range was analyzed. Additionally, the angular luminance profiles of the substrates were evaluated within a display illuminance setup, incorporating a white backlight unit and a conoscope (VCMaster 3D, Eldim), to gauge their performance in practical display environments.

**Mechanical Characterization:** The mechanical properties of the ME were assessed using a universal testing machine (Instron 5655, Instron) equipped with a 1 kN load cell. Test samples, measuring 35 mm by 35 mm with a thickness of 1.1 mm, were prepared for the stretching experiments. The stress-strain curves for each substrate were derived at a stretching speed of 100% per minute. Furthermore, cyclic tests were conducted on the substrates using the same universal testing machine, operating at a stretching speed of 300% per minute within a 30% tensile range. Additionally, to observe the interface between the MM frame and the elastomer matrix under tensile stress, cross-sectional images were acquired using a stretching jig and an optical microscope (BX53M, Olympus).

**LED Array Mounted on Stretchable Substrates:** Commercial green micro-LEDs (Würth Elektronik) were arranged on both the PE and the ME substrates in a 5  $\times$  5 array, with an inter-LED spacing of 7.5 mm. To mitigate undue stress on the connections, copper wires of 0.1 mm diameter were soldered to each LED in an arc shape. An adhesive layer was introduced underneath the LEDs to enhance the bonding characteristics between the LEDs and the substrates. The detailed components for arranging the LED array on a stretchable substrate can be shown in Figure S14 (Supporting Information). The LEDs were powered by applying a direct current voltage. To analyze the displacement of the LED array in the  $x$ - $y$  directions under tensile strain, the stretchable substrate equipped with the LED array was mounted on a custom-built stretching apparatus.

### Supporting Information

Supporting Information is available from the Wiley Online Library or from the author.

### Acknowledgements

J.-C.C. and H.Y.J. contributed equally to this work. This research was supported by the Nano & Material Technology Development Program through the National Research Foundation of Korea (NRF) funded by the Ministry of Science and ICT (RS-2023-00281346) and ICT (RS-2024-00402972).

### Conflict of Interest

The authors declare no conflict of interest.

## Data Availability Statement

The data that support the findings of this study are available on request from the corresponding author. The data are not publicly available due to privacy or ethical restrictions.

## Keywords

image distortion, mechanical metamaterial, stretchable display, zero Poisson's ratio

Received: April 20, 2024

Revised: June 14, 2024

Published online: July 6, 2024

- [1] H. W. Choi, D.-W. Shin, J. Yang, S. Lee, C. Figueiredo, S. Sinopoli, K. Ullrich, P. Jovančić, A. Marrani, R. Momentè, J. Gomes, R. Branquinho, U. Emanuele, H. Lee, S. Y. Bang, S.-M. Jung, S. D. Han, S. Zhan, W. Harden-Chaters, Y.-H. Suh, X.-B. Fan, T. H. Lee, M. Chowdhury, Y. Choi, S. Nicotera, A. Torchia, F. M. Moncunill, V. G. Candel, N. Durães, K. Chang, et al., *Nat. Commun.* **2022**, *13*, 814.
- [2] R. Pode, *Renew. Sust. Energ. Rev.* **2020**, *133*, 110043.
- [3] J. Kim, H. J. Shim, J. Yang, M. K. Choi, D. C. Kim, J. Kim, T. Hyeon, D.-H. Kim, *Adv. Mater.* **2017**, *29*, 1700217.
- [4] J. Park, S. Heo, K. Park, M. H. Song, J.-Y. Kim, G. Kyung, R. S. Ruoff, J.-U. Park, F. Bien, *npj Flex. Electron.* **2017**, *1*, 9.
- [5] T. Yokota, P. Zalar, M. Kaltenbrunner, H. Jinno, N. Matsuhisa, H. Kitanosako, Y. Tachibana, W. Yukita, M. Koizumi, T. Someya, *Sci. Adv.* **2016**, *2*, 1501856.
- [6] J. Yoo, S. Li, D.-H. Kim, J. Yang, M. K. Choi, *Nanoscale Horiz.* **2022**, *7*, 801.
- [7] S.-M. Lee, J. H. Kwon, S. Kwon, K. C. Choi, *IEEE Trans. Electron Devices* **2017**, *64*, 1922.
- [8] E. G. Jeong, J. H. Kwon, K. S. Kang, S. Y. Jeong, K. C. Choi, *J. Inf. Disp.* **2020**, *21*, 19.
- [9] J. H. Koo, D. C. Kim, H. J. Shim, T.-H. Kim, D.-H. Kim, *Adv. Funct. Mater.* **2018**, *28*, 1801834.
- [10] B. Lee, H. Cho, S. Moon, Y. Ko, Y.-S. Ryu, H. Kim, J. Jeong, S. Chung, *Nat. Electron.* **2023**, *6*, 1.
- [11] Y. Lee, J. W. Chung, G. H. Lee, H. Kang, J.-Y. Kim, C. Bae, H. Yoo, S. Jeong, H. Cho, S.-G. Kang, J. Y. Jung, D.-W. Lee, S. Gam, S. G. Hahm, Y. Kuzumoto, S. J. Kim, Z. Bao, Y. Hong, Y. Yun, S. Kim, *Sci. Adv.* **2021**, *7*, eabg9180.
- [12] M. S. Lim, M. Nam, S. Choi, Y. Jeon, Y. H. Son, S.-M. Lee, K. C. Choi, *Nano Lett.* **2020**, *20*, 1526.
- [13] H. Cho, B. Lee, D. Jang, J. Yoon, S. Chung, Y. Hong, *Mater. Horiz.* **2022**, *9*, 2053.
- [14] D. Yin, N.-R. Jiang, Z.-Y. Chen, Y.-F. Liu, Y.-G. Bi, X.-L. Zhang, J. Feng, H.-B. Sun, *Adv. Opt. Mater.* **2020**, *8*, 1901525.
- [15] Y. Lee, B. J. Kim, L. Hu, J. Hong, J.-H. Ahn, *Mater. Today* **2022**, *53*, 51.
- [16] C. Du, Y. Wang, Z. Kang, *ACS Appl. Mater. Interfaces* **2023**, *15*, 19190.
- [17] J. Liu, J. Wang, Z. Zhang, F. Molina-Lopez, G.-J. N. Wang, B. C. Schroeder, X. Yan, Y. Zeng, O. Zhao, H. Tran, T. Lei, Y. Lu, Y.-X. Wang, J. B.-H. Tok, R. Dauskardt, J. W. Chung, Y. Yun, Z. Bao, *Nat. Commun.* **2020**, *11*, 3362.
- [18] M. W. Jeong, J. H. Ma, J. S. Shin, J. S. Kim, G. Ma, T. U. Nam, X. Gu, S. J. Kang, J. Y. Oh, *Sci. Adv.* **2023**, *9*, eadh1504.
- [19] D. C. Kim, H. J. Shim, W. Lee, J. H. Koo, D.-H. Kim, *Adv. Mater.* **2020**, *32*, 1902743.
- [20] Z. Zhang, W. Wang, Y. Jiang, Y.-X. Wang, Y. Wu, J.-C. Lai, S. Niu, C. Xu, C.-C. Shih, C. Wang, H. Yan, L. Galuska, N. Prine, H.-C. Wu, D. Zhong, G. Chen, N. Matsuhisa, Y. Zheng, Z. Yu, Y. Wang, R. Dauskardt, X. Gu, J. B.-H. Tok, Z. Bao, *Nature* **2022**, *603*, 624.
- [21] B. Jang, S. Won, J. Kim, J. Kim, M. Oh, H.-J. Lee, J.-H. Kim, *Adv. Funct. Mater.* **2022**, *32*, 2113299.
- [22] G. N. Greaves, A. L. Greer, R. S. Lakes, T. Rouxel, *Nat. Mater.* **2011**, *10*, 823.
- [23] Y.-J. Lee, S.-M. Lim, S.-M. Yi, J.-H. Lee, S. Kang, G.-M. Choi, H. N. Han, J.-Y. Sun, I.-S. Choi, Y.-C. Joo, *Extreme Mech. Lett.* **2019**, *31*, 100516.
- [24] Z. Wang, C. Luan, G. Liao, J. Liu, X. Yao, J. Fu, *Adv. Eng. Mater.* **2020**, *22*, 2000312.
- [25] M. Wallbanks, M. F. Khan, M. Bodaghi, A. Triantaphyllou, A. Serjouei, *Smart Mater. Struct.* **2021**, *31*, 023002.
- [26] J. Huang, Q. Zhang, F. Scarpa, Y. Liu, J. Leng, *Compos. B: Eng.* **2017**, *110*, 72.
- [27] L. L. Hu, Z. J. Wu, M. H. Fu, *Int. J. Mech. Sci.* **2018**, *140*, 537.
- [28] J. N. Grima, L. Mizzi, K. M. Azzopardi, R. Gatt, *Adv. Mater.* **2016**, *28*, 385.
- [29] D. Paretar, X. Xu, C.-Y. Hui, A. Jagota, *Soft Matter* **2014**, *10*, 4084.
- [30] Y. Wang, Y. Cai, H. Zhang, J. Zhou, S. Zhou, Y. Chen, M. Liang, H. Zou, *Polymer* **2021**, *236*, 124299.
- [31] A. Zahid, B. Dai, R. Hong, D. Zhang, *Mater. Res. Express* **2017**, *4*, 105301.
- [32] M. A. Eddings, M. A. Johnson, B. K. Gale, *J. Micromech. Microeng.* **2008**, *18*, 067001.
- [33] N. Amouroux, L. Léger, *Langmuir* **2003**, *19*, 1396.